Bi-regional dynamic contrast-enhanced MRI for prediction of microvascular invasion in solitary BCLC stage A hepatocellular carcinoma

ELECTRONIC SUPPLEMENTARY MATERIAL

Appendix E1 MR imaging acquisition protocol

The conventional liver MRI protocols at our institution includes the following sequence: (1) breath-hold axial fat-suppressed T1-weighted gradient recalled echo images including in-phase and opposed-phase acquired with three-dimensional (3D) liver acquisition with volume acceleration flexible (LAVA-Flex) sequences; (2) breath-hold coronal single-shot fast spin-echo T2-weighted imaging (T2WI); (3) respiratory-triggered axial PROPELLER T2-weighted imaging with fat suppression (T2WI/FS); and (4) respiratory-triggered axial diffusion weighted imaging (DWI) sequence included two *b* values (*b* values = 0 and 800 s/mm^2). Quantitative DCE-MRI was performed by using multiphase axial 3D spoiled-gradient recalled-echo sequences for liver acquisition with volume acceleration-extended volume (LAVA-XV) sequence with breath-hold. According to our previous study [1], pre-contrast T1 mapping with four different flip angles (3°, 6°, 9°, and 12°) was acquired before dynamic scanning for the determination of pre-contrast T1 values. Then a dynamic scan with 42 consecutive phases was performed, which shared the scanning parameters and range as T1 mapping, with a flip angle of 15° and temporal resolution of 4-6 s/phase. A bolus of gadodiamide (Omniscan 0.5 mmol/mL; GE Healthcare, Ireland) was injected using a standard dosage of 0.1 mmol/kg at a rate of 3.0 mL/s though an automated power injector, followed by flushing of 20 mL saline at the same rate. The intermittent breath holding method was adopted during DCE sequence scanning: every three consecutive phases were acquired in one breath hold with a break of 5–8 s for each cycle and repeated for 14 cycles. The total scanning time for DCE-MRI was 4–5 min. At last, a coronal LAVA-Flex sequence was acquired.

References:

1. Zhu Y, Zhou Y, Zhang W, Xue L, Li Y, Jiang J, et al (2021) Value of quantitative dynamic contrast-enhanced and diffusion-weighted magnetic resonance imaging in predicting extramural venous invasion in locally advanced gastric cancer and prognostic significance. Quant Imaging Med Surg 11(1):328-34

Appendix E2 Perfusion DCE-MR image processing

The multi-phase DCE MR images were registered by GenIQ software package on Advantage Workstation version 4.7 (GE Healthcare, USA) for pre-processing prior to further analysis. The registered DCE-MR images were processed and analyzed using an inhouse program written on MATLAB R2018a (MathWorks, Natick, MA, USA). First, two round region of interest (ROI) was manually placed on abdominal aorta and main portal vein at level of porta hepatis for arterial input function (AIF) and portal vein input function (VIF) calculation, which were used as an estimation for the hepatic arterial and portal venous blood supply, respectively. Then, a third ROI was manually traced along the edge of the liver at the slice of maximum tumor diameter. The signal intensity on MRI was converted into an equivalent concentration of contrast material using multiple flip angles method and T1 fitting. Subsequently, the contrast concentration curves of the ROIs were calculated using a dual-input single compartment model, which depicts contrast material distribution after injection and predicts a change in the contrast concentration in the tissue as a function of time, C(t), using the below equation according to previously described [1, 2]:

$$\frac{dC(t)}{dt} = k_{1a} \cdot C_a(t) + k_{1p} \cdot C_p(t) - k_2 \cdot C(t)$$

where $C(t)$, $C_a(t)$, and $C_p(t)$ were the concentrations of contrast material in the tissue, aorta, and portal vein, and, respectively; k_{1a}, k_{1p}, and k_2 were constants for the aortic inflow rate, the portal venous inflow rate, and the outflow rate, respectively.

References:

1. Stocker D, Hectors S, Bane O, Vietti-Violi N, Said D, Kennedy P, et al (2021) Dynamic contrast-enhanced MRI perfusion quantification in hepatocellular carcinoma: comparison of gadoxetate disodium and gadobenate dimeglumine. Eur Radiol 31(12):9306-9315
2. Hectors SJ, Wagner M, Besa C, Bane O, Dyvorne HA, Fiel MI, et al (2016) Intravoxel incoherent motion diffusion-weighted imaging of hepatocellular carcinoma: Is there a correlation with flow and perfusion metrics obtained with dynamic contrast-enhanced MRI? J Magn Reson Imaging 44(4):856-864

Table S1. MR imaging acquisition protocol and main sequence parameters

Sequence	Plane	TR (ms)	TE (ms)	FOV (mm)	Matrix	FA (degrees)	ST/gap (mm)	NEX	Bandwidth (kHz)	Acquisition time
LAVA-Flex T1WI	Axial	5.1	1.4	400	288×224	12	5/0	1	166.67	14 (s)
SS-FSE T2WI	Coronal	1816	68	400	288×288	90	4/1	1	83.33	45 (s)
FS T2WI Propeller	Axial	8,000-10,000	96-100	400	320×320	90	5/1	2.5	50.0	3-4 (min)
SS-EPI DWI *	Axial	8000-10,000	56-60	380	128×160	90	5/1	2	250	1.50 (min)
Precontrast LAVA-XV T1WI	Axial	2.9	1.4	380	288×224	3, 6, 9, and 12	5/0	1	125	6 (s)
DCE-perfusion MRI	Axial	2.9	1.4	380	288×224	15	5/0	1	125	4-6 (min)
Postcontrast LAVA-	Coronal	4.2	1.9	400×36	352×25	15	4/0	1	200	16 (s)

Flex T1WI	0	6

* Acquired using respiratory trigger technique and 2 *b*-values were used (0 and 800 s/mm^2)

DCE, dynamic-contrast enhanced; *DWI*, diffusion-weighted imaging; *FA*, Flip angle; *FOV*, Field of view; *FS*, fat suppression; *LAVA-Flex*, liver acquisition with volume acceleration; *LAVA-XV*, liver acquisition with volume acceleration-extended volume; *NEX*, number of excitations; *SS-EPI*, Single-shot echo-planar imaging; *SS-FSE*, single-shot fast-recovery fast spin-echo; *ST*, slice thickness; *T1WI*, T1-weighted imaging; *T2WI*, T2-weighted imaging; *TE*, echo time; *TR*, repetition time

Table S2. Definition of each MR imaging feature in this study

MR imaging feature	Definitions
LI-RADS major features [1]	
Tumor size, cm	Largest outer-edge-to-outer-edge dimension of an observation.
No-rim arterial phase hyperenhancement	Nonrim-like enhancement in arterial phase unequivocally greater in whole or in part than liver.
Non-peripheral washout	Nonperipheral visually assessed temporal reduction in enhancement in whole or in part relative to composite liver tissue from earlier to later phase resulting in hypoenhancement in the extracellular phase.
Enhancing capsule	Smooth, uniform, sharp border around most or all of an observation, unequivocally thicker or more conspicuous than fibrotic tissue around background nodules, and visible as enhancing rim in PVP, DP, or TP.
LI-RADS ancillary features (favoring HCC in particular)	
Non-enhancing capsule	Capsule appearance not visible as an enhancing rim.
Nodule-in-nodule architecture	Presence of smaller inner nodule within and having different imaging features than larger outer nodule.
Mosaic architecture	Presence of randomly distributed internal nodules or compartments, usually with different imaging features.
Fat in mass, more than adjacent liver	Relative paucity of fat in solid mass compared to steatotic liver OR in inner nodule relative to steatotic outer nodule.
Blood products in mass	Intralesional hemorrhage in absence of biopsy, trauma, or intervention. Perilesional hemorrhage

	may or may not be present.
LI-RADS ancillary features (favoring malignancy, not HCC in particular)	
Restricted diffusion	Intensity on DWI, not attributable solely to T2 shine-through, unequivocally higher than liver and/or ADC unequivocally lower than liver
Mild-moderate T2 hyperintensity	Signal intensity on T2-weighted images mildly or moderately higher than liver and similar to or less than non-iron-overloaded spleen
Corona enhancement	Periobservational enhancement in late arterial phase or early PVP attributable to venous drainage from tumor.
Fat sparing in solid mass	Relative paucity of fat in solid mass compared to steatotic liver OR in inner nodule relative to steatotic outer nodule
Iron sparing in solid mass	Paucity of iron in solid mass relative to iron-overloaded liver or in inner nodule relative to outer siderotic nodule.
Non-LIRADS imaging features	
Cirrhosis	Imaging manifestations of cirrhosis including morphological alteration (global atrophy, segmental volume redistribution, and regional or focal parenchymal contraction), parenchymal alteration (parenchymal nodules, fibrotic scars surrounding parenchymal nodules, confluent hepatic fibrosis, nonspecific parenchymal heterogeneity, fat, and iron accumulation), vascular alterations (hepatic artery, portal vein, and intrahepatic veins, etc.), biliary alterations (peribiliarycysts), functional alterations in HBP (altered expression levels of hepatocyte transporters), musculoskeletal manifestations (sarcopenia), and portal hypertension (portal-systemic collaterals, spleen, fluid retention, submucosal edema) [1].

Tumor margin	Defined on the portal venous phase and/or delayed phase, and was categorized as i) smooth margin presenting as nodular tumors with smooth contour, and ii) non-smooth margin presenting as an irregular margin that had budding portion at the tumor periphery protruding into the liver parenchyma [2].
Tumor capsule	A thin, linear and hyperenhancement structure surrounded the tumor border in the portal venous and/or delayed phase and grouped into absent, incomplete, and intact types [3].
TTPVI	The presence of internal arteries visible in the arterial phase and the absence of hypointense halo in a post-arterial phase [4].

Note—Unless otherwise indicated, all MR imaging features were defined according to the LI-RADS version 2018 [1]

ADC, apparent diffusion coefficient; *DP*, delayed phase; *DWI*, diffusion-weighted imaging; *HBP*, hepatobiliary phase; *HCC*, hepatocellular carcinoma; *LI-RADS*, Liver Imaging Reporting and Data System; *PVP*, portal venous phase; *TP*, transitional phase; *TTPVI*, two-trait predictor of venous invasion

References:

1. American College of Radiology website. CT/MRI LI-RADS v2018. www.acr.org/Clinical-Resources/Reporting-and-Data-Systems/LI-RADS/CT-MRI-LI-RADSv2018.Accessed January 2021
2. Dong SY, Wang WT, Chen XS, Yang YT, Zhu S, Zeng MS, et al. Microvascular invasion of small hepatocellular carcinoma can be preoperatively predicted by the 3D quantification of MRI. Eur Radiol 2022;32(6):4198-4209.
3. Liu B, Zeng Q, Huang J, Zhang J, Zheng Z, Liao Y, et al. IVIM using convolutional neural networks predicts microvascular invasion in HCC. Eur Radiol 2022;32(10):7185-7195.
4. Renzulli M, Brocchi S, Cucchetti A, Mazzotti F, Mosconi C, Sportoletti C, et al. Can Current Preoperative Imaging Be Used to Detect Microvascular Invasion of Hepatocellular Carcinoma? Radiology 2016;279(2):432-442.

Table S3. Interobserver variability for DCE perfusion quantitative parameters measurement of primitive lesions in patients with hepatocellular carcinoma

DCE perfusion parameters	ICC	95% Confidence Interval	*P* value
Intra-tumoral region			
ART (%)	0.932	0.883 – 0.982	< 0.001
Fa (ml/min/100 g)	0.886	0.824 – 0.944	< 0.001
Fp (ml/min/100 g)	0.905	0.863 – 0.970	< 0.001
Ft (ml/min/100 g)	0.887	0.842 – 0.933	< 0.001
DV (%)	0.953	0.922 – 0.985	< 0.001
MTT (sec)	0.894	0.832 – 0.942	< 0.001
Peritumoral region			
ART (%)	0.874	0.835 – 0.918	< 0.001
Fa (ml/min/100 g)	0.825	0.783 – 0.877	< 0.001
Fp (ml/min/100 g)	0.804	0.753 – 0.860	< 0.001
Ft (ml/min/100 g)	0.893	0.844 – 0.951	< 0.001
DV (%)	0.864	0.803 – 0.924	< 0.001
MTT (sec)	0.858	0.821 – 0.889	< 0.001

ART, arterial fraction; *DCE*, dynamic-contrast enhanced; *DV*, distribution volume; F_a, arterial blood flow; F_p, portal venous blood flow; F_t, total blood flow; *ICC*, intraclass correlation coefficient; *MTT*, mean transit time

Table S4. Inter-observer agreement for radiological characteristics

Features	Reader 1	Reader 2	Disagreement	Kappa (95 % CI) *	
LI-RADS major features					
Tumor size, cm			0	1.000	(1.000, 1.000)
< 2.0	0	0			
≥ 2.0	133	133			
No-rim arterial phase hyperenhancement			7	0.734	(0.607, 0.861)
Absent	7	9			
Present	126	124			
Non-peripheral washout			6	0.864	(0.758, 0.970)
Absent	27	29			
Present	106	104			
Enhancing capsule			12	0809	(0.705, 0.913)
Absent	51	49			
Present	83	85			
LI-RADS ancillary features (favoring HCC in particular)					
Non-enhancing capsule			7	0.770	(0.607, 0.933)
Absent	116	115			
Present	17	18			
Nodule-in-nodule architecture			6	0.674	(0.431, 0.917)
Absent	114	112			
Present	9	11			
Mosaic architecture			13	0.794	(0.688, 0.900)
Absent	83	80			
Present	50	53			
Fat in mass, more than adjacent liver			16	0.695	(0.556, 0.834)
Absent	98	96			
Present	35	37			
Blood products in mass			15	0.701	(0.562, 0.840)
Absent	102	97			
Present	31	36			
LI-RADS ancillary features (favoring malignancy, not HCC in particular)					
Restricted diffusion			0	1.000	(1.000, 1.000)
Absent	0	0			
Present	133	133			

Mild-moderate T2 hyperintensity			0	1.000	(1.000, 1.000)
Absent	0	0			
Present	133	133			
Corona enhancement			11	0.807	(0.699, 0.915)
Absent	91	92			
Present	42	41			
Fat sparing in solid mass			5	0.762	(0.562, 0.962)
Absent	121	122			
Present	12	11			
Iron sparing in solid mass			3	0.716	(0.410, 1.000)
Absent	128	127			
Present	5	6			
Non-LIRADS imaging features					
Cirrhosis			11	0.834	(0.740, 0.928)
Absent	70	73			
Present	63	60			
Tumor margin			12	0.806	(0.702, 0.910)
Smooth	83	85			
Non-smooth	50	48			
Tumor capsule			11	0.825	(0.727, 0.923)
Complete	80	85			
Incomplete/absent	53	48			
TTPVI			7	0.874	(0.784, 0.964)
Absent	92	95			
Present	41	38			

Except where indicated otherwise, data are expressed as numbers with percentages in parentheses

* Data are expressed as kappa coefficient with 95% CIs in parentheses

CI, confidence interval; *HCC*, hepatocellular carcinoma; *LI-RADS*, Liver Imaging Reporting and Data System; *TTPVI*, two-trait predictor of venous invasion

Table S5. Construction of clinic-radiological, DCE, and combined models through multivariate logistic analysis

Models *	β	S.E.	Wald	*P* value	OR	95% CI for OR	
						Lower	Upper
Clinic-radiological model							
AFP, ng/ml							
≤ 20 vs. 20~400	1.622	0.669	5.880	0.015	5.064	1.365	18.788
≤ 20 vs. > 400	2.675	0.781	11.722	< 0.001	14.517	3.139	67.148
Corona enhancement (Present)	1.471	0.557	6.969	0.008	4.355	1.461	12.983
TTPVI (Present)	1.685	0.605	7.767	0.005	5.395	1.649	17.652
Constant							
Intra-tumoral model							
F_t (ml/min/100 g)	0.048	0.010	25.343	<0.001	1.049	1.030	1.069
MTT (sec)	-0.167	0.075	4.972	0.026	0.846	0.731	0.980
Constant	-2.123	1.098	3.741	0.053			
Peritumoral model							
ART (%)	0.171	0.044	12.927	< 0.001	1.186	1.088	1.293

Constant	-5.407	1.267	18.222	< 0.001	0.004		
DCE model							
F_t-T (mL/min/100 g)	0.026	0.009	7.950	0.005	1.026	1.008	1.004
ART-P (%)	0.170	0.048	12.761	< 0.001	1.185	1.080	1.301
Constant	-10.052	2.308	18.966	< 0.001	0.000		
Combined model							
AFP, ng/mL							
≤ 20 vs. 20~400	2.346	1.028	5.206	0.023	10.446	1.392	78.386
≤ 20 vs. > 400	4.630	1.352	11.726	< 0.001	102.554	7.244	1451.885
Corona enhancement (Present)	2.394	0.916	6.825	0.009	10.957	1.818	66.021
TTPVI (Present)	3.291	1.213	7.369	0.007	26.880	2.497	289.410
C_{DCE}	1.315	0.343	14.683	< 0.001	3.726	1.901	7.300
Constant	-4.079	1.116	13.356	< 0.001	0.017		

[*] A stepwise forward method was used to assess the best independent predictor of microvascular invasion

AFP, alpha fetoprotein; *ART*, arterial fraction; *β*, coefficient; C_{DCE}, combined quantitative parameter of DCE-MRI; *CI*, confidence interval; *DCE*, dynamic-contrast enhanced; F_t, total blood flow; *MTT*, mean transit time; *OR*, odds ratio; *P*, peritumoral region; *S.E.*, standard error; *T*, intra-tumoral region; *TTPVI*, two-trait predictor of venous invasion

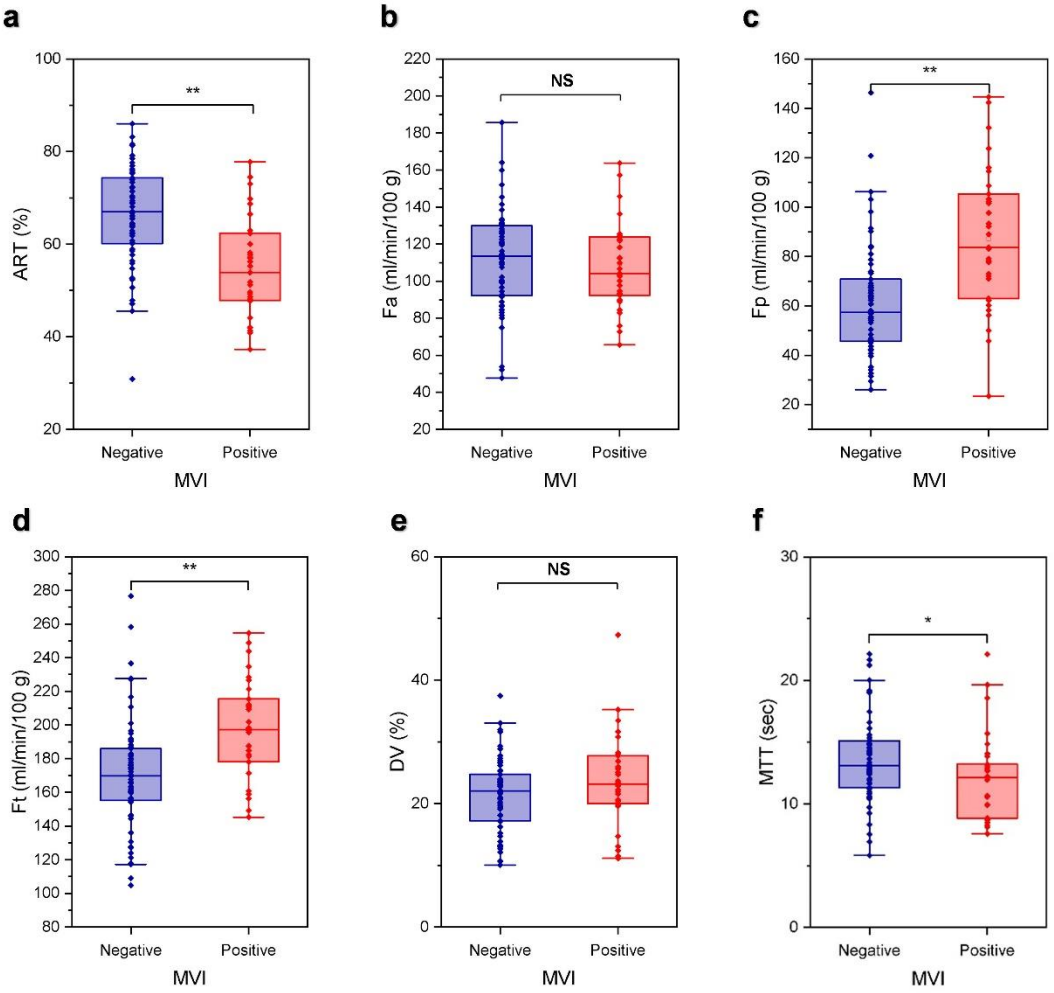

Fig. S1. Box and whisker plots of the show the distribution of each perfusion DCE parameter of intra-tumoral region in the training set between MVI positive and MVI negative groups. Box and whisker plots of ART (**a**), F_a (**b**), F_p (**c**), F_t (**d**), DV (**e**) and MTT (**f**) between MVI positive and MVI negative groups, respectively. Boxes show the upper and lower quartiles, and horizontal lines within boxes indicate median values, whiskers indicate first quartile minus 1.5 times inner quartile range and third quartile plus 1.5 times inner quartile range, and circles indicate outliers. Asterisks indicate significant differences between MVI positive and MVI negative groups ($P < 0.05$). NS indicate no significant differences between MVI positive and MVI negative groups ($P > 0.05$). *MVI*, microvascular invasion.

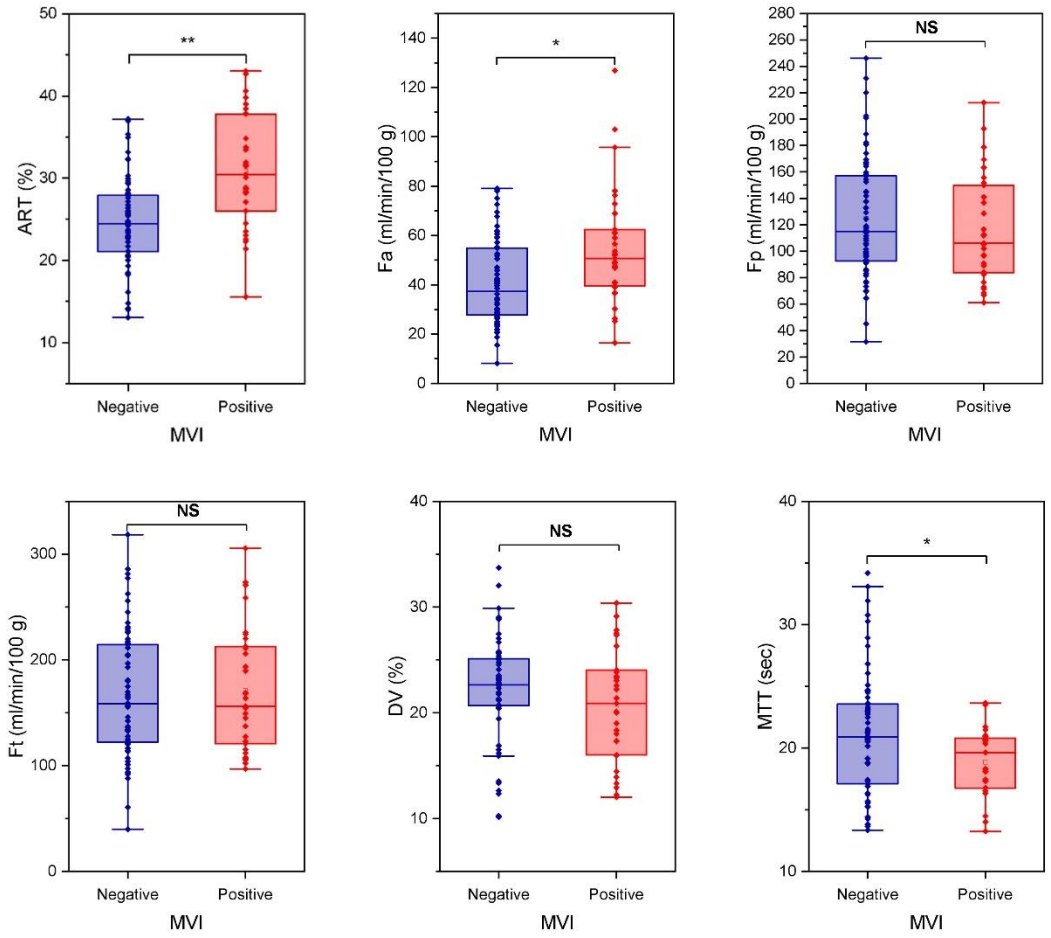

Fig. S2. Box and whisker plots of the show the distribution of each perfusion DCE parameter of peri-tumoral region in the training set between MVI positive and MVI negative groups. Box and whisker plots of ART (**a**), F_a (**b**), F_p (**c**), F_t (**d**), DV (**e**) and MTT (**f**) between MVI positive and MVI negative groups, respectively. Boxes show the upper and lower quartiles, and horizontal lines within boxes indicate median values, whiskers indicate first quartile minus 1.5 times inner quartile range and third quartile plus 1.5 times inner quartile range, and circles indicate outliers. Asterisks indicate significant differences between MVI positive and MVI negative groups ($P < 0.05$). NS indicate no significant differences between MVI positive and MVI negative groups ($P > 0.05$). *MVI*, microvascular invasion.

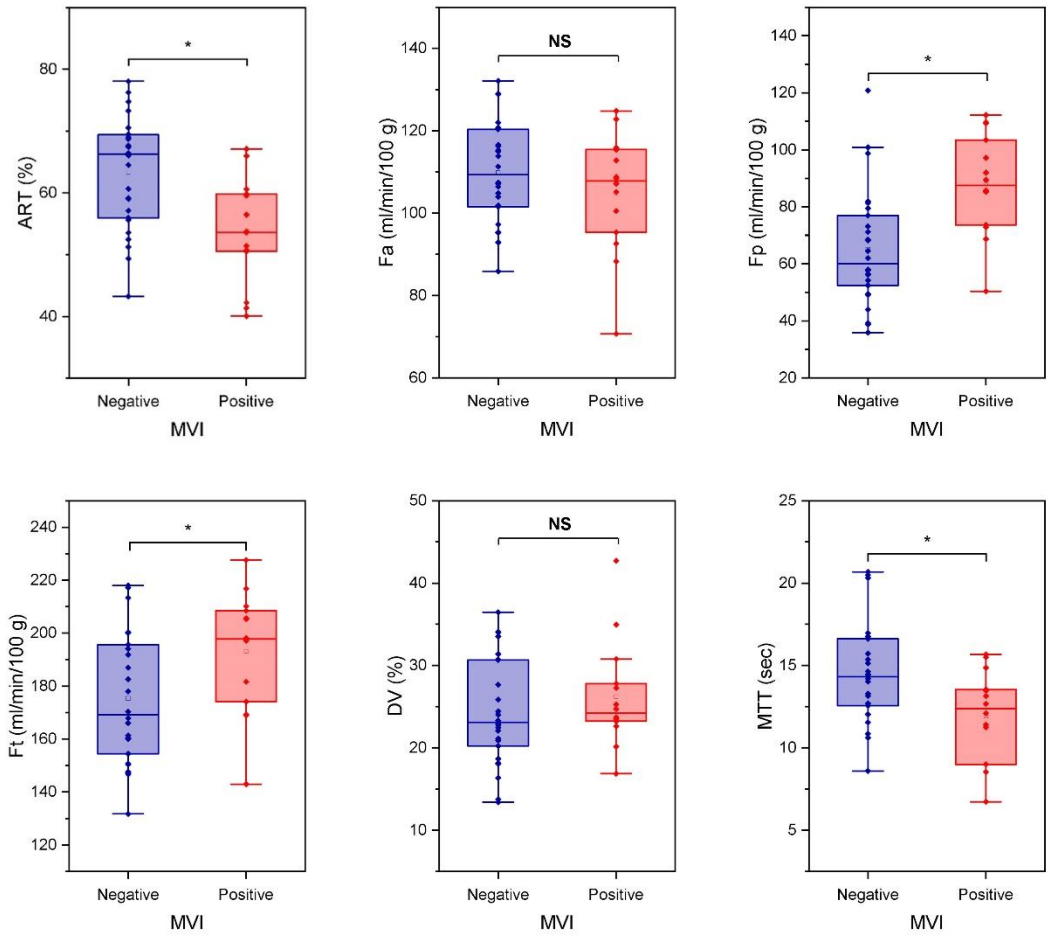

Fig. S3. Box and whisker plots of the show the distribution of each perfusion DCE parameter of intra-tumoral region in the validation set between MVI positive and MVI negative groups. Box and whisker plots of ART (**a**), F_a (**b**), F_p (**c**), F_t (**d**), DV (**e**) and MTT (**f**) between MVI positive and MVI negative groups, respectively. Boxes show the upper and lower quartiles, and horizontal lines within boxes indicate median values, whiskers indicate first quartile minus 1.5 times inner quartile range and third quartile plus 1.5 times inner quartile range, and circles indicate outliers. Asterisks indicate significant differences between MVI positive and MVI negative groups ($P < 0.05$). NS indicate no significant differences between MVI positive and MVI negative groups ($P > 0.05$). *MVI*, microvascular invasion.

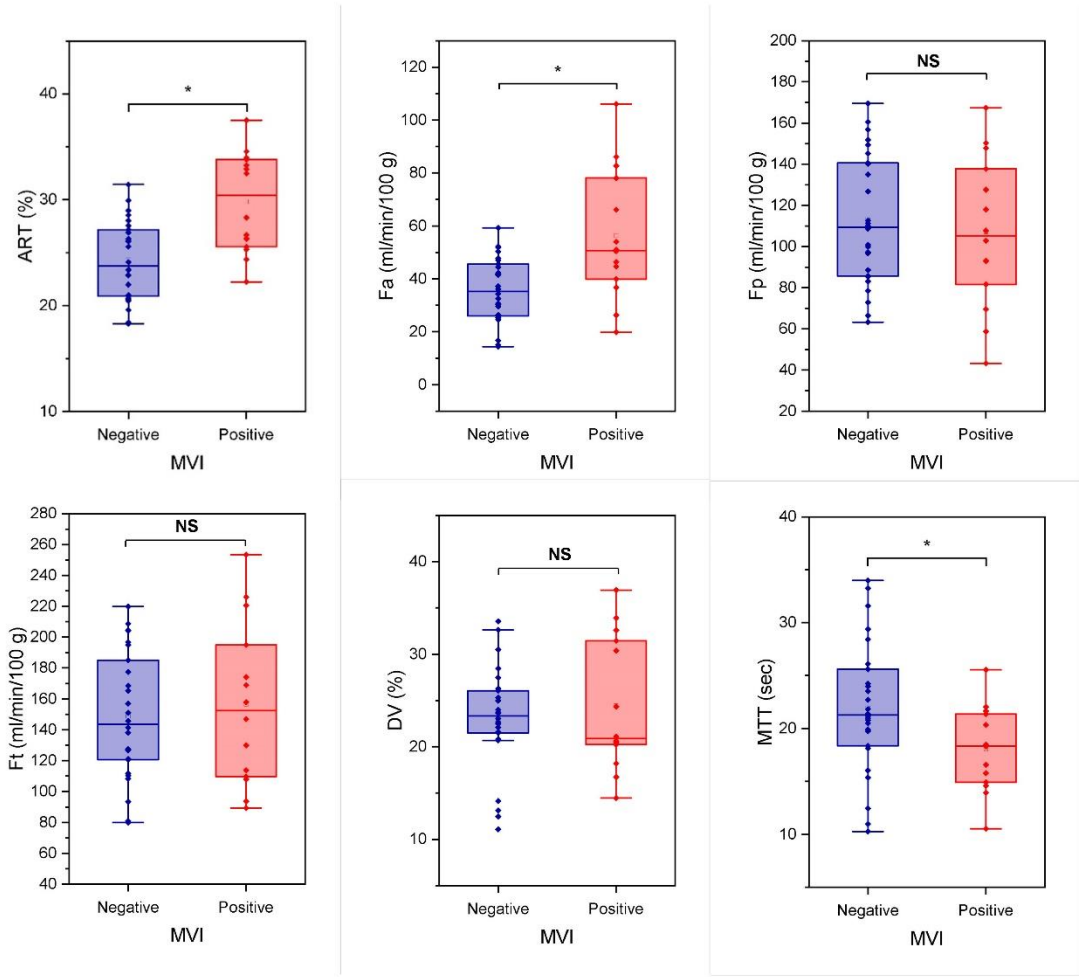

Fig. S4. Box and whisker plots of the show the distribution of each perfusion DCE parameter of peri-tumoral region in the validation set between MVI positive and MVI negative groups. Box and whisker plots of ART (**a**), F_a (**b**), F_p (**c**), F_t (**d**), DV (**e**) and MTT (**f**) between MVI positive and MVI negative groups, respectively. Boxes show the upper and lower quartiles, and horizontal lines within boxes indicate median values, whiskers indicate first quartile minus 1.5 times inner quartile range and third quartile plus 1.5 times inner quartile range, and circles indicate outliers. Asterisks indicate significant differences between MVI positive and MVI negative groups ($P < 0.05$). NS indicate no significant differences between MVI positive and MVI negative groups ($P > 0.05$). *MVI*, microvascular invasion.

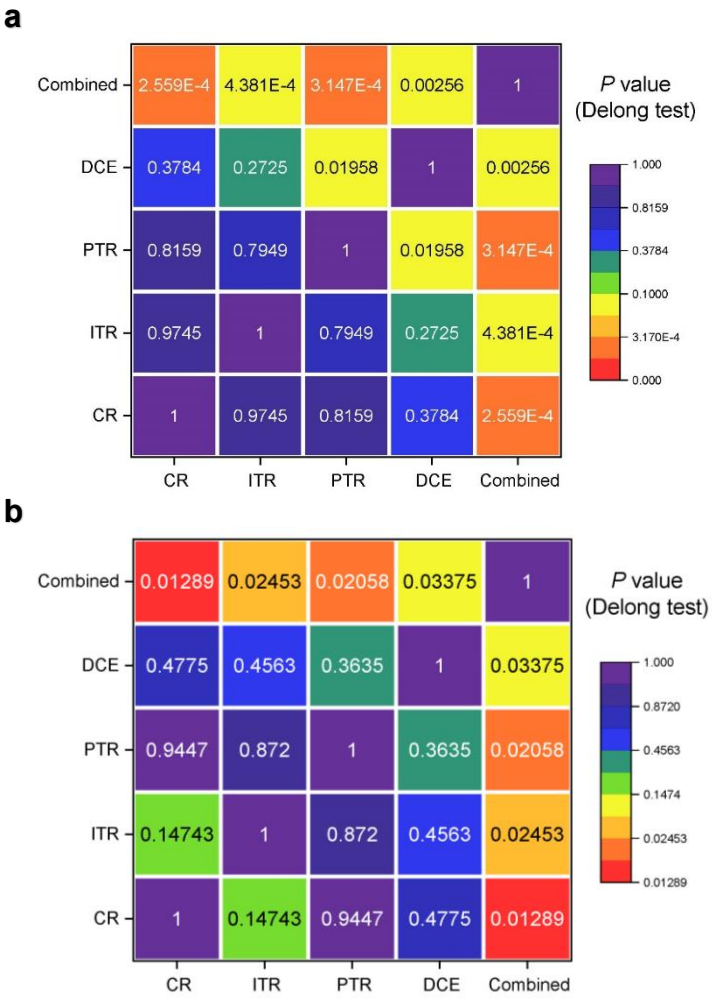

Fig. S5. Heat maps show the *p* values of the Delong test used for comparing the areas under the curves of different predicting models for microvascular invasion in hepatocellular carcinoma. *CR*, clinic-radiological; *DCE*, dynamic-contrast enhanced; *ITR*, intra-tumoral region; *PTR*, peritumoral region